Volume 17 | Number 27 | 21 July 2015 | Pages 4961–5118

CrystEngComm

www.rsc.org/crystengcomm

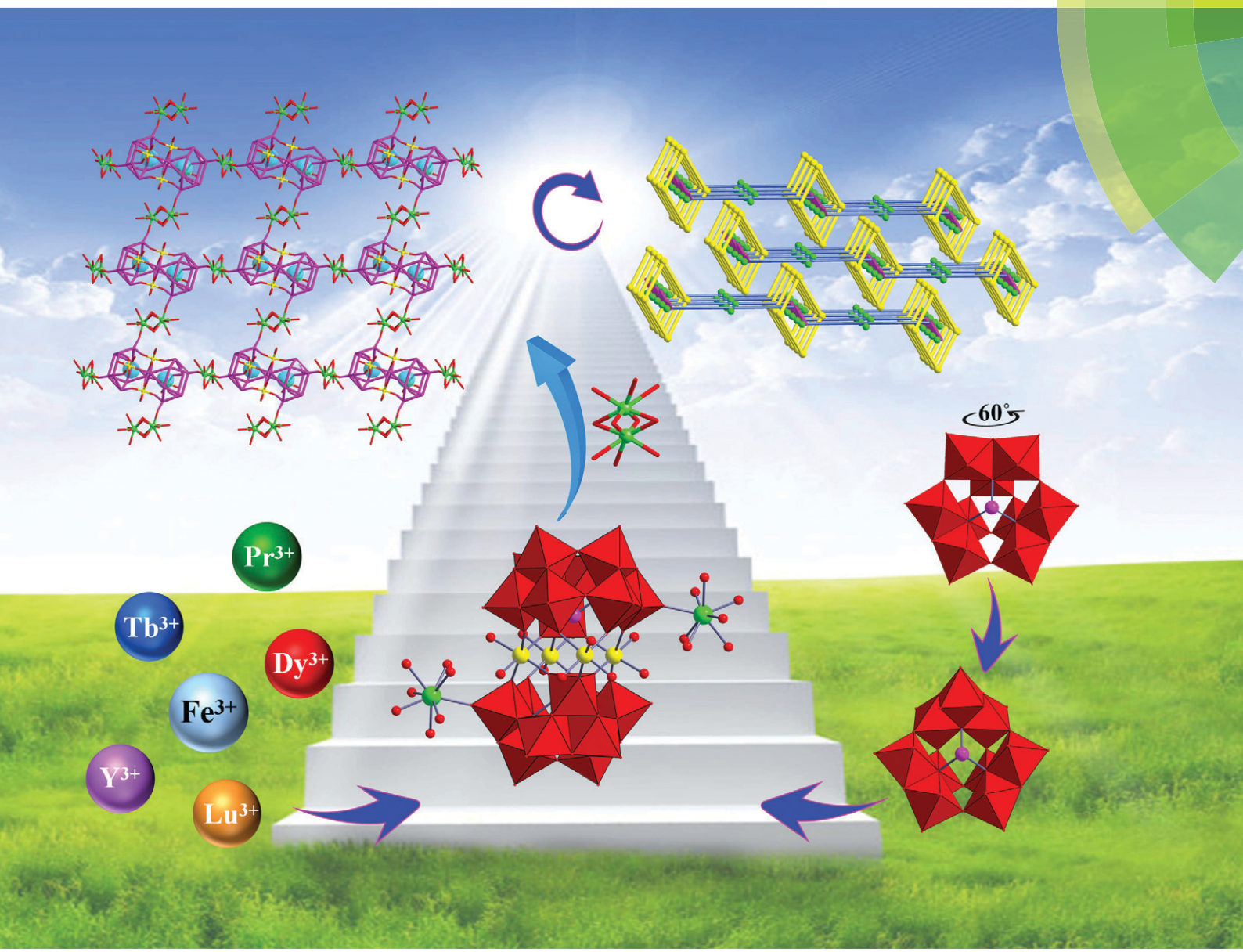

ROYAL SOCIETY OF CHEMISTRY

PAPER

Jie Luo, Junwei Zhao *et al.*

The first purely inorganic polyoxotungstates constructed from dimeric tungstoantimonate-based iron–rare-earth heterometallic fragments

CrystEngComm

PAPER

Cite this: *CrystEngComm*, 2015, **17**, 5002

The first purely inorganic polyoxotungstates constructed from dimeric tungstoantimonate-based iron–rare-earth heterometallic fragments†

Lijuan Chen, Jing Cao, Xinghua Li, Xing Ma, Jie Luo* and Junwei Zhao*

The rational self-assembly of a trilacunary Keggin precursor with Fe^{3+} and RE^{3+} (rare-earth) ions *via* a conventional aqueous solution method has led to a series of novel tungstoantimonate-based Fe–RE heterometallic derivatives $[Pr(H_2O)_8][Pr(H_2O)_6][Fe_4(H_2O)_{10}(B\text{-}\beta\text{-}SbW_9O_{33})_2]\cdot 16H_2O$ (**1**) and $[RE(H_2O)_7]_2[Fe_4(H_2O)_{10}(B\text{-}\beta\text{-}SbW_9O_{33})_2]\cdot 22H_2O$ [RE = Tb^{III} (**2**), Dy^{III} (**3**), Lu^{III} (**4**), Y^{III} (**5**)], which have been further structurally characterized by elemental analysis, IR spectroscopy, powder X-ray diffraction (PXRD), single-crystal X-ray diffraction and thermogravimetric (TG) analysis. To the best of our knowledge, **1–5** represent the first purely inorganic Fe–RE heterometallic tungstoantimonates based on the trilacunary Keggin $[B\text{-}\beta\text{-}SbW_9O_{33}]^{9-}$ unit. In **1**, the tetra-Fe^{III} substituted sandwich-type unit $[Fe_4(H_2O)_{10}(B\text{-}\beta\text{-}SbW_9O_{33})_2]^{6-}$ is built up of two trilacunary Keggin subunits $[B\text{-}\beta\text{-}SbW_9O_{33}]^{9-}$ sandwiching a rhomb-like $\{Fe^{III}_4\}$ cluster, and then the disordered Pr^{III} cations work as bridges that link adjacent sandwich-type units $[Fe_4(H_2O)_{10}(B\text{-}\beta\text{-}SbW_9O_{33})_2]^{6-}$, giving rise to the first 2-D extended sheet based on tungstoantimonate fragments and Fe–RE heterometallic cations. **2–5** are isomorphic and exhibit a discrete structure composed of a tetra-Fe^{III} substituted sandwich-type unit $[Fe_4(H_2O)_{10}(B\text{-}\beta\text{-}SbW_9O_{33})_2]^{6-}$ and two supporting $[RE(H_2O)_8]^{3+}$ cations. The electrochemical and electrocatalytic properties of **1** and **2** have been investigated in detail in a 0.5 mol L^{-1} $Na_2SO_4 + H_2SO_4$ supporting electrolyte, and both **1** and **2** illustrate obvious electrocatalytic activity toward the reduction of NO_2^- and BrO_3^-.

Received 31st March 2015,
Accepted 12th May 2015

DOI: 10.1039/c5ce00633c

www.rsc.org/crystengcomm

Introduction

It is well known that the featured oxygen-enriched surfaces, high negative charges and controllable sizes of lacunary polyoxometalate (POM) precursors derived from several classic polyoxoanions (POAs), such as the Keggin type $\{XM_{12}O_{40}\}$, Dawson type $\{X_2M_{18}O_{62}\}$, and Lindqvist type $\{M_6O_{19}\}$, are the reasons why they are often recommended as excellent multidentate inorganic ligands that link various transition-metal (TM) or rare-earth (RE) cations into novel polynuclear functional aggregates with diverse metal nuclearities, beautiful structural topologies and unique properties.[1] Among the well-known class of TM or RE containing POM aggregates, the sandwich-type POM-based derivatives have been widely explored. Within the class of those species, the sandwich-type species constructed from two trivacant Keggin $[\alpha\text{-}XW_9O_{34}]^{9/10-}$ (X = Si^{IV}, Ge^{IV}, P^V, As^V) or Dawson $[\alpha\text{-}X_2W_{15}O_{56}]^{12-}$ (X = P^V, As^V) fragments and a TM core probably represent the best known and most studied subfamily since the first rhomb-like tetra-Co^{II} substituted sandwich-type species $[Co_4(H_2O)_2(B\text{-}\alpha\text{-}PW_9O_{34})_2]^{10-}$ was reported by Weakley *et al.* in 1973.[2] The existence of Sb^{III}-containing POMs has been known for a long time,[3] and most of the published findings are based on the trivacant Keggin $[SbW_9O_{33}]^{9-}$ fragment. Among these tungstoantimonates (TAs), a majority of them are dimeric sandwich-type structures constructed from two trivacant Keggin $[SbW_9O_{33}]^{9-}$ fragments encapsulating a metal cluster. In 1997, Krebs *et al.* firstly reported the synthesis approaches of the $[B\text{-}\alpha\text{-}SbW_9O_{33}]^{9-}$ POA and the dimeric Krebs-type sandwich $[Sb_2W_{22}O_{74}(OH)_2]^{12-}$ POA,[4] where the $[Sb_2W_{22}O_{74}(OH)_2]^{12-}$ POA is composed of two trivacant Keggin-type segments $[B\text{-}\beta\text{-}SbW_9O_{33}]^{9-}$ joined *via* a sandwich belt of two interior $\{WO_2\}^{2+}$ and two exterior $\{WO(OH)_2\}^{2+}$ groups. Subsequently, Krebs and co-workers showed that two exterior $\{WO(OH)_2\}^{2+}$ moieties can be substituted by extraneous $\{M(H_2O)_3\}^{2+/3+}$ fragments, leading to the TM-substituted $[Sb_2W_{20}M_2O_{70}(H_2O)_6]^{n-}$ POAs (M = Fe^{III}, Co^{II}, Mn^{II}, Ni^{II}, Cu^{II}, Zn^{II}).[5,6] From then on, the continuous interest in exploring TM-substituted Krebs-type TAs has persisted and the rate of discovering novel derivatives has been steadily growing. As we know, the groups of Proust, Kortz, Bi and Wang all

Henan Key Laboratory of Polyoxometalate Chemistry, Institute of Molecular and Crystal Engineering, College of Chemistry and Chemical Engineering, Henan University, Kaifeng, Henan 475004, PR China. E-mail: luojie@henu.edu.cn, zhaojunwei@henu.edu.cn

† Electronic supplementary information (ESI) available: Additional data. CSD 429364–429368 for 1–5. See DOI: 10.1039/c5ce00633c

demonstrated that two exterior $\{WO(OH)_2\}^{2+}$ moieties of this structure-type can be easily replaced by organometallic groups forming novel organometallic derivatives such as $[Sb_2W_{20}O_{70}\{Ru(p\text{-cymene})\}_2]^{10-}$,[7] $[Sb_2W_{20}O_{70}(RuC_6H_6)_2]^{10-}$,[8] $[Sb_2W_{20}O_{70}(RuC_{10}H_{14})_2]^{10-}$,[8] $[Sb_2W_{20}Ru_2(H_2O)_2(dmso)_6O_{68}]^{4-}$,[9] and $[\{Sn(C_4H_6O_2)(H_2O)\}_2(WO_2)_2(B\text{-}\beta\text{-}SbW_9O_{33})_2]^{10-}$.[10] On the other hand, Kortz *et al.* also showed that adamantane-like $\{Ru_4O_6(H_2O)_9\}^{4+}$ cluster units were able to take the place of two terminal $\{WO(OH)_2\}^{2+}$ groups.[11] Furthermore, Hill's group prepared two Krebs-type metal carbonyl complexes $Na_{11}H[Sb_2W_{20}O_{70}\{Re(CO)_3\}_2]\cdot 34H_2O$ and $K_9Na_3[Sb_2W_{20}O_{70}\{Mn(CO)_3\}_2]\cdot 32H_2O$,[12] in which two tricarbonyl $\{M(CO)_3\}^+$ cations substitute two $\{WO(OH)_2\}^{2+}$ moieties on the Krebs-type POM skeleton. Later, Kortz evidenced that two inner and two outer W centers in the Krebs-type TA can be substituted by TM cations, resulting in $[M_4(H_2O)_{10}(B\text{-}\beta\text{-}SbW_9O_{33})_2]^{6-}$ (M = Fe^{III}, Al^{III}).[13,14] Very recently, Reinoso *et al.* also obtained a series of organic functionalization derivatives of TM-substituted Krebs-type POMs $[\{M(imc)(H_2O)\}_2(WO_2)_2(B\text{-}\beta\text{-}SbW_9O_{33})_2]^{12-}$ (M = Mn^{II}, Co^{II}, Ni^{II}, Zn^{II}) and $[(2,3\text{-pyzdc})_2\{NaNi_2(H_2O)_4Sb_2W_{20}O_{70}\}_2]^{22-}$.[15] Meanwhile, the other structure types of TM-substituted derivatives based on trilacunary $[SbW_9O_{33}]^{9-}$ fragments have also been reported. Some representative examples are listed here: Cronin *et al.* isolated a monotitanium embedded POA $[Na_5TiO(B\text{-}\alpha\text{-}SbW_9O_{33})_2]^{11-}$, which is composed of two $[B\text{-}\alpha\text{-}SbW_9O_{33}]^{9-}$ fragments linked by five sodium ions and a unique square pyramidal $Ti(O)O_4$ group.[16] Pope *et al.* synthesized a di-UO_2^{2+} sandwiched TA $[(UO_2)_2(H_2O)_2(SbW_9O_{33})_2]^{14-}$.[17] A number of Hervé-type trinuclear substituted sandwich-type TAs were also discovered by several groups with various metal nuclearities (Cu^{II}, Zn^{II}, Mn^{II}, Co^{II}, Ni^{II}, Pd^{II}).[18] And a unique hexanuclear substituted sandwich-type TA $[(MnCl)_6(B\text{-}\alpha\text{-}SbW_9O_{33})_2]^{12-}$ was communicated by Yamase and co-workers.[19a] Moreover, Hill's group reported a molecular highly unusual feature tetramer $[\{Na(\mu\text{-}OH_2)(OH_2)_2\}_6\{Sn_6(B\text{-}SbW_9O_{33})_2\}_2]^{6-}$.[19b] In contrast to TM-substituted TAs, there are few reports on RE-substituted TAs including an unprecedented Ce^{III}-containing derivative $[(SbW_9O_{33})_4\{WO_2(H_2O)\}_2Ce_3(H_2O)_8(Sb_4O_4)]^{19-}$,[20] a Y^{III}-containing trimer $[\{Y(\alpha\text{-}SbW_9O_{31}(OH)_2)(CH_3COO)(H_2O)\}_3(WO_4)]^{17-}$ that is composed of three $[\alpha\text{-}SbW_9O_{33}]^{9-}$ segments linked by three Y^{III} ions and a capping, tetrahedral WO_4^{2-} group,[21] and two inorganic sandwich-type dimers $[RE(H_2O)_4Sb_2W_{21}O_{72}(OH)]^{10-}$ (RE = Yb^{III}, Lu^{III}) and $[RE_2(H_2O)_8(Sb_2W_{20}O_{70})]^{8-}$ (RE = Yb^{III}, Lu^{III}, Y^{III}).[22] However, to our knowledge, the research on TM–RE heterometallic TAs containing the trilacunary $[SbW_9O_{33}]^{9-}$ fragments remains largely undeveloped. Under this background, we have isolated a family of organic–inorganic hybrid TM–RE heterometallic TAs with amino acid ligands $[RE(H_2O)_8]_2[Fe_4(H_2O)_8(thr)_2][B\text{-}\beta\text{-}SbW_9O_{33}]_2\cdot 22H_2O$ (RE = Pr^{III}, Nd^{III}, Sm^{III}, Eu^{III}, Gd^{III}, Dy^{III}, Lu^{III}).[23] As a part of our continuous work, herein, we report a series of $[B\text{-}\beta\text{-}SbW_9O_{33}]^{9-}$-based 3d–4f heterometallic purely inorganic POMs $[Pr(H_2O)_8][Pr(H_2O)_6][Fe_4(H_2O)_{10}(B\text{-}\beta\text{-}SbW_9O_{33})_2]\cdot 16H_2O$ (**1**) and $[RE(H_2O)_7]_2[Fe_4(H_2O)_{10}][B\text{-}\beta\text{-}SbW_9O_{33}]_2\cdot 22H_2O$ (RE = Tb^{III} (**2**), Dy^{III} (**3**), Lu^{III} (**4**), Y^{III} (**5**)). Their common characteristic is that they comprise a tetra-Fe^{III} substituted sandwich-type unit $[Fe_4(H_2O)_{10}(B\text{-}\beta\text{-}SbW_9O_{33})_2]^{6-}$ with the bonding RE ingredients on their surface. **1** displays the 2-D extended sheet constructed from the tetra-Fe^{III} substituted sandwich-type units $[Fe_4(H_2O)_{10}(B\text{-}\beta\text{-}SbW_9O_{33})_2]^{6-}$ through Pr^{III} linkers, whereas the molecular structures of **2**–**5** consist of a tetra-Fe^{III} substituted sandwich-type unit $[Fe_4(H_2O)_{10}(B\text{-}\beta\text{-}SbW_9O_{33})_2]^{6-}$ and two supporting $[RE(H_2O)_8]^{3+}$ cations. As far as we know, **1**–**5** stand for the first purely inorganic TM–RE heterometallic TAs. The electrochemical and electrocatalytic properties of **1** and **2** have been investigated in detail.

Experimental

Materials and physical measurements

The trilacunary precursor $Na_9[B\text{-}\alpha\text{-}SbW_9O_{33}]\cdot 19.5H_2O$ was synthesized as previously described[4] and further identified by IR spectroscopy. All other reagents were used as purchased without further purification. Hydrogen elemental analysis was performed on a Perkin-Elmer 2400-II CHNS/O analyzer. Inductively coupled plasma atomic emission spectrometry (ICP-AES) was performed using a Perkin-Elmer Optima 2000 ICP-AES spectrometer. IR spectra were recorded with a Nicolet FT-IR 360 spectrometer using KBr pellets in the range of 4000–400 cm^{-1}. Powder X-ray diffraction (PXRD) patterns were collected using a Bruker D8 ADVANCE instrument with Cu Kα radiation (λ = 1.54056 Å). Cyclic voltammograms were recorded on a CS electrochemical workstation (Wuhan CorrTest Instrument Co. Ltd) at room temperature. Twice-distilled water was used throughout the experiments. A conventional three-electrode system was used. The working electrode was a glassy carbon, a platinum gauze was used as a counter electrode and an Ag/AgCl electrode was referenced. The supporting electrolyte of **1** and **2** was 0.5 mol L^{-1} Na_2SO_4 + H_2SO_4 aqueous solution. TG analyses were carried out under a N_2 atmosphere using a Mettler–Toledo TGA/SDTA 851e instrument with a heating rate of 10 °C min^{-1} from 25 to 750 °C.

Preparations of 1–7

$[Pr(H_2O)_8][Pr(H_2O)_6][Fe_4(H_2O)_{10}(B\text{-}\beta\text{-}SbW_9O_{33})_2]\cdot 16H_2O$ (1). $Na_9[B\text{-}\alpha\text{-}SbW_9O_{33}]\cdot 19.5H_2O$ (0.200 g, 0.070 mmol), $FeCl_3\cdot 6H_2O$ (0.032 g, 0.118 mmol), and $PrCl_3\cdot 6H_2O$ (0.070 g, 0.197 mmol) were dissolved in 15 mL of water with stirring and the pH value of the solution was carefully adjusted to 0.5 using a dilute HCl solution (4 mol L^{-1}). The solution was stirred for 2 h, heated at 80 °C for 2 h and then filtered when it cooled to room temperature. Slow evaporation of the filtrate at room temperature led to green yellow cubic block crystals of **1** for several days. Yield: *ca.* 33% (based on $FeCl_3\cdot 6H_2O$). Anal. calcd. (found %) for $H_{80}Fe_4O_{106}Pr_2Sb_2W_{18}$ (**1**): H 1.38 (1.57), Fe 3.83 (3.71), Pr 4.83 (4.66), Sb 4.17 (4.38), W 56.72 (56.59). IR (KBr pellets, cm^{-1}): 3393(vs), 1634(s), 957(m), 889(w), 777(vs), 662(m), 472(w), 418(w).

$[Tb(H_2O)_7]_2[Fe_4(H_2O)_{10}][B\text{-}\beta\text{-}SbW_9O_{33}]_2\cdot 22H_2O$ (2). The synthesis process of **2** is similar to **1**, except that $TbCl_3\cdot 6H_2O$ (0.070 g, 0.187 mmol) replaced $PrCl_3\cdot 6H_2O$. Yield: *ca.* 30% (based on $FeCl_3\cdot 6H_2O$). Anal. calcd. (found %) for $H_{92}Fe_4O_{112}Sb_2W_{18}Tb_2$ (**2**): H 1.55 (1.64), Fe 3.74 (3.64), Tb 5.32 (5.40), Sb 4.07 (4.00), W 55.35 (55.45). IR (KBr pellets, cm^{-1}): 3397(vs), 1643(s), 953(m), 883(w), 783(vs), 649(m), 474(w), 421(w).

$[Dy(H_2O)_7]_2[Fe_4(H_2O)_{10}][B\text{-}\beta\text{-}SbW_9O_{33}]_2\cdot 22H_2O$ (3). The synthesis process of **3** is similar to **1**, except that $DyCl_3\cdot 6H_2O$ (0.100 g, 0.265 mmol) replaced $PrCl_3\cdot 6H_2O$. Yield: *ca.* 35% (based on $FeCl_3\cdot 6H_2O$). Anal. calcd. (found %) for $H_{92}Fe_4O_{112}Sb_2W_{18}Tb_2$ (**3**): H 1.55 (1.64), Fe 3.74 (3.64), Dy 5.32 (5.40), Sb 4.07 (4.00), W 55.35 (55.45). IR (KBr pellets, cm^{-1}): 3413(vs), 1632(s), 952(m), 878(w), 788(vs), 660(m), 469(w), 421(w).

$[Lu(H_2O)_7]_2[Fe_4(H_2O)_{10}][B\text{-}\beta\text{-}SbW_9O_{33}]_2\cdot 22H_2O$ (4). The synthesis process of **4** is similar to **1**, except that $LuCl_3\cdot 6H_2O$ (0.070 g, 0.180 mmol) replaced $PrCl_3\cdot 6H_2O$. Yield: *ca.* 38% (based on $FeCl_3\cdot 6H_2O$). Anal. calcd. (found %) for $H_{92}Fe_4O_{112}Sb_2W_{18}Lu_2$ (**4**): H 1.54 (1.65), Fe 3.72 (3.60), Lu 5.82 (5.71), Sb 4.05 (3.94), W 55.05 (55.17). IR (KBr pellets, cm^{-1}): 3407(vs), 1638(s), 952(m), 889(w), 782(vs), 655(m), 474(w), 421(w).

$[Y(H_2O)_7]_2[Fe_4(H_2O)_{10}][B\text{-}\beta\text{-}SbW_9O_{33}]_2\cdot 22H_2O$ (5). The synthesis process of **5** is similar to **1**, except that $YCl_3\cdot 6H_2O$ (0.100 g, 0.330 mmol) replaced $PrCl_3\cdot 6H_2O$. Yield: *ca.* 36% (based on $FeCl_3\cdot 6H_2O$). Anal. calcd. (found %) for $H_{92}Fe_4O_{112}Sb_2W_{18}Y_2$ (**5**): H 1.59 (1.67), Fe 3.83 (3.74), Y 3.05 (3.16), Sb 4.17 (4.29), W 56.68 (56.59). IR (KBr pellets, cm^{-1}): 3392(vs), 1633(s), 953(m), 883(w), 776(vs), 660(m), 474(w), 415(w).

X-ray crystallography

Intensity data for **1–5** were collected on a Bruker APEX-II CCD diffractometer using graphite monochromatized Mo Kα radiation (λ = 0.71073 Å) at 296(2) K. Direct methods were used to solve their structures and locate the heavy atoms using the SHELXTL-97 program package.[24] The remaining atoms were found from successive full-matrix least-squares refinements on F^2 and Fourier syntheses. Routine Lorentz polarization and empirical absorption corrections were applied. No hydrogen atoms associated with water molecules were located from the difference Fourier map. All non-hydrogen atoms were refined anisotropically except for some oxygen atoms and water molecules. It should be pointed out that the Pr1 and Pr2 cations are disordered over two positions with the site occupancy of 50% for each position. Similar disordered phenomenon has been observed in the previous document.[25a] Crystal data and structure refinements for **1–5** were summarized in Table 1. The CCDC reference numbers for **1–5** are 429364–429368, respectively. These data can be obtained from the Fachinformationszentrum Karlsruhe, 76344 Eggenstein-Leopoldshafen, Germany (fax: +49 7247 808 666; e-mail: crysdata@fiz-karlsruhe.de).

Results and discussion

Synthesis

Over the past several decades, a number of POM-based TM–RE heterometallic derivatives (PTRHDs) have been successfully synthesized, leading to a growing family of PTRHDs with an intriguing variety of architectures and topologies, since the first series of PTRHDs $[RE(H_2O)_5\{Ni(H_2O)\}_2As_4W_{40}O_{140}]^{21-}$ (RE = Y^{III}, Ce^{III}, Pr^{III}, Nd^{III}, Sm^{III}, Eu^{III}, Gd^{III})

Table 1 Crystallographic data and structural refinements for **1–5**

	1	**2**	**3**	**4**	**5**
Formula	$H_{80}Fe_4O_{106}Sb_2W_{18}Pr_2$	$H_{92}Fe_4O_{112}Sb_2W_{18}Tb_2$	$H_{92}Fe_4O_{112}Sb_2W_{18}Dy_2$	$H_{92}Fe_4O_{112}Sb_2W_{18}Lu_2$	$H_{92}Fe_4O_{112}Sb_2W_{18}Y_2$
M_r (g mol^{-1})	5834.66	5978.78	5985.94	6010.88	5838.60
T (K)	296(2)	296(2)	296(2)	296(2)	296(2)
Crystal system	Triclinic	Triclinic	Triclinic	Triclinic	Triclinic
Space group	$P\bar{1}$	$P\bar{1}$	$P\bar{1}$	$P\bar{1}$	$P\bar{1}$
a (Å)	12.7448(10)	12.7304(5)	12.7569(12)	12.7131(16)	12.7178(5)
b (Å)	12.7563(9)	13.0108(5)	13.0680(12)	12.9743(17)	13.0050(5)
c (Å)	16.1414(12)	15.9909(6)	16.0200(15)	15.960(2)	15.9829(6)
α (deg)	78.1290(10)	75.3150(10)	75.2730(10)	75.090(2)	75.2040(10)
β (deg)	74.3740(10)	74.3990(10)	74.4050(10)	75.892(6)	74.3750(10)
γ (deg)	83.6220(10)	76.0750(10)	75.9710(10)	75.818(2)	75.9460(10)
V (Å^3)	2468.9(3)	2425.05(16)	2444.0(4)	2405.1(5)	2418.00(16)
Z	1	1	1	1	1
D_c (g cm^{-3})	3.924	4.094	4.067	4.150	4.010
μ (mm^{-1})	23.059	23.938	23.834	24.718	23.751
No. of reflections collected	12 495	12 450	12 172	12 121	12 372
No. of independent reflections	8478	8447	8355	8369	8416
R_{int}	0.0389	0.0358	0.0455	0.0339	0.0495
Limiting indices	$-15 \le h \le 14$	$-15 \le h \le 15$	$-13 \le h \le 15$	$-14 \le h \le 15$	$-9 \le h \le 15$
	$-15 \le k \le 11$	$-10 \le k \le 15$	$-15 \le k \le 15$	$-10 \le k \le 15$	$-15 \le k \le 15$
	$-19 \le l \le 18$	$-19 \le l \le 18$	$-18 \le l \le 18$	$-18 \le l \le 18$	$-19 \le l \le 18$
GOF on F^2	1.007	1.043	1.013	1.017	1.029
R_1, wR_2 [$I > 2\sigma(I)$]	0.0522, 0.1337	0.0365, 0.0923	0.0503, 0.1271	0.0432, 0.1106	0.0549, 0.1450
R_1, wR_2 [all data]	0.0613, 0.1393	0.0399, 0.0942	0.0566, 0.1312	0.0522, 0.1157	0.0599, 0.1493

were published by Xue *et al.* in 2004.[25b] However, the preparation of novel PTRHDs has been a great challenge because the pH stability region for TM cations in aqueous solutions is different from that of RE cations; furthermore, there are unavoidable competitive reactions among highly negative POM precursors, strongly oxyphilic RE ions and less active TM ions in the same reaction system.[26] Consequently, it is comparatively difficult to seek suitable reaction conditions that would capacitate the acquisition of novel PTRHD aggregates. In order to further explore novel extended aggregates in this domain with the "property-adding" feature, an effective strategy was developed to utilize the lacunary POAs as inorganic polydentate building units to capture TM and RE ions for constructing the extended PTRHD multifunctional hybrid materials. Highly lacunary POM precursors are selected as the ideal candidates because of their nucleophilic oxygen-enriched surfaces and high negative charges, which allow incorporation of more metal centers.[27] It should be pointed out that the choice of diverse "connectors" such as TM cations or RE cations is important since they can effectively link lacunary POM precursors. As far as we know, since the first extended inorganic PTRHD was discovered by Wang's group in 2007,[28] hitherto, more than twenty extended PTRHDs have been obtained by means of various TM or RE linkers (Table 2).[29] In Table 2, it was evident that only seven examples of extended PTRHDs with RE linkers have been reported. In 2007, Wang *et al.* reported the first 1-D chiral ladder-like chain based on tetra-Mn^{III} substituted $[Mn_4Si_2W_{18}O_{68}(H_2O)_2]^{12-}$ units and Ce^{3+} linkers.[27] Subsequently, the first 2-D inorganic aggregate $K_3Na_3\{Nd_2(H_2O)_{12}Cu_4(H_2O)_2(SiW_9O_{34})_2\}\cdot 21H_2O$ built by tetra-Cu^{II} sandwiched $[Cu_4(H_2O)_2(SiW_9O_{34})_2]^{12-}$ units and Nd^{3+} linkers was also obtained by them.[29b] In 2010, Mailane *et al.* reported a 1-D double-chain system $Cs_4[(\gamma\text{-}SiW_{10}O_{36})_2(Cr(OH)(H_2O))_3(La(H_2O)_7)_2]_3\cdot 19H_2O$, in which sandwich-type $[(\gamma\text{-}SiW_{10}O_{36})_2(Cr(OH)(H_2O))_3]^{10-}$ moieties were connected by La^{3+} cations.[29g] In 2012, Niu's group obtained a 1-D helical chain formed by $[\alpha\text{-}SiW_{11}O_{39}]^{8-}$ POAs and RE^{3+} cations, which was further extended to a 3-D framework through Cu^{2+} cations. Recently, Yang and coworkers discovered the first 3-D Mn–Ce heterometallic organic–inorganic hybrid framework $K_4Na_4[Ce_2(ox)_3(H_2O)_2]_2\{[Mn(H_2O)_3]_2[(Mn_4GeW_9O_{34})_2(H_2O)_2]\}\cdot 14H_2O$ constructed by sandwich-type TM-substituted POAs and mixed 3d and 4f metal linkers.[29p] They also synthesized two 3-D frameworks $KNa_7[\{Sm_6Mn(\mu\text{-}H_2O)_2(OCH_2COO)_7(H_2O)_{18}\}\{Na(H_2O)P_5W_{30}O_{110}\}]\cdot 22H_2O$ and $K_4[\{Sm_4Cu_2(gly)_2(ox)(H_2O)_{24}\}\{NaP_5W_{30}O_{110}\}]Cl_2\cdot 25H_2O$ that contain $\{P_5W_{30}\}$ units and TM/RE–carboxylate–RE connectors.[29q] It is obvious that only three examples of extended purely inorganic PTRHDs have been reported. On the other hand, the exploration on purely inorganic TM–RE heterometallic TAs remains largely undeveloped. This background provides us with an excellent opportunity to exploit the TA–TM–RE system. Eventually, we have successfully obtained a novel 2-D purely inorganic TM–RE heterometallic TA $[Pr(H_2O)_8][Pr(H_2O)_6][Fe_4(H_2O)_{10}(B\text{-}\beta\text{-}SbW_9O_{33})_2]\cdot 16H_2O$ (1) and four 0-D purely inorganic TM–RE heterometallic TAs $[RE(H_2O)_7]_2[Fe_4(H_2O)_{10}][B\text{-}\beta\text{-}SbW_9O_{33}]_2\cdot 22H_2O$ [RE = Tb^{III} (2), Dy^{III} (3), Lu^{III} (4), Y^{III} (5)]. In the beginning, 1 was first obtained by reaction of $Na_9[B\text{-}\alpha\text{-}SbW_9O_{33}]\cdot 19.5H_2O$, $FeCl_3\cdot 6H_2O$ and $PrCl_3\cdot 6H_2O$ in an aqueous solution, pH = 0.5, at 80 °C. And then the

Table 2 The summary of extended POM-based TM–RE heterometallic materials

Year	Dimension	Linkers	Phase
2007	1-D	Ce^{3+}	$K_4Na_2[\{Ce(H_2O)_7\}_2Mn_4Si_2W_{18}O_{68}(H_2O)_2]\cdot 21.5H_2O$[27]
2008	1-D	Cu^{2+}	$K_2H_7[\{RE(PW_{11}O_{39})_2\}\{Cu_2(bpy)_2(\mu\text{-}ox)\}]\cdot xH_2O$[29a]
	2-D	Nd^{3+}	$K_3Na_3\{Nd_2(H_2O)_{12}Cu_4(H_2O)_2(SiW_9O_{34})_2\}\cdot 21H_2O$[29b]
2009	1-D	Cu^{2+}	$[H_9\{Ce(\alpha\text{-}PW_{11}O_{39})_2\}Cu(en)_2]\ 6H_2O$[29c]
	2-D	Cu^{2+}	$[Cu(en)_2][(Cu(en)(OH))_3La(SiW_{11}O_{39})]\cdot 20H_2O$[29d]
2010	1-D	Cu^{2+}	$H_2[Cu(en)_2H_2O]_8[Cu(en)_2]_3[\{(\alpha\text{-}SiW_{11}O_{39})Ce(H_2O)(\eta^2,\mu\text{-}1,1)CH_3COO\}_4]\cdot 22H_2O$[29e]
	1-D	Cu^{2+}	$H_8[Cu(en)_2H_2O]_4[Cu(en)_2]\{[Cu(en)_2][La(PW_{11}O_{39})_2]\}_2\cdot 18H_2O$[29f]
	1-D	La^{3+}	$Cs_4[(\gamma\text{-}SiW_{10}O_{36})_2(Cr(OH)(H_2O))_3(La(H_2O)_7)_2]_3\cdot 19H_2O$[29g]
2011	1-D	Cu^{2+}	$\{[Cu(en)_2]_{1.5}[Cu(en)(2,2'\text{-bipy})(H_2O)n]RE[(\alpha\text{-}PW_{11}O_{39})_2]\}_6$ (RE = Ce, Pr)[29h]
	2-D	Cu^{2+}	$\{[Cu(en)_2]_2(H_2O)[Cu(en)(2,2'\text{-bipy})]RE[(\alpha\text{-}HPW_{11}O_{39})_2]\}_4$ (RE = Gd, Tb, Er)[29h]
	3-D	Cu^{2+}	$\{[Cu(en)_2]_{1.5}[Cu(en)(2,2'\text{-bipy})]Nd[(\alpha\text{-}H_5PW_{11}O_{39})_2]\}_3$[29h]
	2-D	Cu^{2+}	$[Cu(en)_2]_2H_6[Ce(\alpha\text{-}PW_{11}O_{39})_2]\cdot 8H_2O$[29i]
	2-D	Cu^{2+}	$[Cu(dap)_2(H_2O)][Cu(dap)_2]_{4.5}[Dy(\alpha\text{-}PW_{11}O_{39})_2]\cdot 4H_2O$[29i]
	2-D	Cu^{2+}	$[Cu(dap)(H_2O)_2]_{0.5}[Cu(dap)_2]_4H_2[Pr(\alpha\text{-}PW_{11}O_{39})_2]\cdot 3H_2O$[29j]
2012	3-D	Fe^{3+}	$[\varepsilon\text{-}PMo^{V}{}_8Mo^{VI}{}_4O_{37}(OH)_3\{La(H_2O)_5(Fe(CN)_6)_{0.25}\}_4]\cdot 12H_2O$[29k]
	1-D	K^+	$K(enH_2)_4[Cu(en)_2(H_2O)]_2\{[Cu(en)_2]_{1.5}Gd[(\alpha\text{-}H_{1.75}SiW_{11}O_{39})_2]\}_2\cdot\sim 15H_2O$[29l]
	3-D	RE^{3+}, Cu^{2+}	$(enH_2)_{0.5}\{[Cu(en)_2]_{1.5}\ RE[(\alpha\text{-}HSiW_{11}O_{39})]\}\cdot 3H_2O$ (RE = La, Ce)[29l]
	3-D	Cu^{2+}	$(enH_2)_2\{[Cu(en)_2(H_2O)][Cu(en)_2]_2RE[(\alpha\text{-}H_{1.5}SiW_{11}O_{39})_2]\}\cdot 6H_2O$ (RE = Pr, Sm)[29l]
	1-D	Cu^{2+}	$[Cu(en)_2(H_2O)]_2\{[Cu(en)_2]_2[Cu(pzda)_2][(\alpha\text{-}H_2SiW_{11}O_{39})Ce(H_2O)]_2\}\cdot n\ H_2O$[29m]
	1-D	Cu^{2+}	$[Cu(dap)(H_2O)_2]_{0.5}[Cu(dap)_2(H_2O)]_2[Cu(dap)_2]_3[RE(\alpha\text{-}AsW_{11}O_{39})_2]\cdot xH_2O$ (RE = Pr, Eu)[29n]
	2-D	Cu^{2+}	$[Cu(dap)_2]_{5.5}[RE(\alpha\text{-}AsW_{11}O_{39})_2]\cdot xH_2O$ (RE = Tb, Dy)[29n]
	2-D	Cu^{2+}	$Na[Cu(en)_2(H_2O)]_4[Cu(en)_2]_2[Cu(H_2O)_4]_{0.5}\{Cu(en)_2[H_2Ce^{IV}(\alpha\text{-}AsW_{11}O_{39})_2]_2\}\cdot 10H_2O$[29n]
	2-D	Cu^{2+}	$Na_3[Cu(en)_2(H_2O)][Cu(en)_2]_{1.5}[H_3\ RE(\alpha\text{-}AsW_{11}O_{39})_2]\cdot xH_2O$ (RE = Pr, Nd, Sm, Eu, Tb)[29n]
2013	3-D	Mn^{2+}, Ce^{3+}	$K_4Na_4[Ce_2(ox)_3(H_2O)_2]_2\{[Mn(H_2O)_3]_2[Mn_4(GeW_9O_{34})_2(H_2O)_2]\}\cdot 14H_2O$[29o]
	1-D	Cu^{2+}	$[Cu(en)_2(H_2O)][Cu(en)_2][Tb(\alpha\text{-}PW_{11}O_{39})(H_2O)_2(ox)Cu(en)]\cdot 6H_2O$[29p]
2014	3-D	Mn^{2+}, Sm^{3+}	$KNa_7[\{Sm_6Mn(\mu\text{-}H_2O)_2(OCH_2COO)_7(H_2O)_{18}\}\{Na(H_2O)P_5W_{30}O_{110}\}]\cdot 22H_2O$[29q]
	3-D	Mn^{2+}, Sm^{3+}	$K_4[\{Sm_4Cu_2(gly)_2(ox)(H_2O)_{24}\}\{NaP_5W_{30}O_{110}\}]Cl_2\cdot 25H_2O$[29q]

replacement of the Pr^{III} cation by Tb^{III}, Dy^{III}, Lu^{III}, Y^{III} cations led to the formation of 2–5. 1 exhibited a 2-D sheet architecture while 2–5 are isolated structures. These results imply that the nature of RE cations may influence the structural diversity of the products. Moreover, investigations on other RE cations in this system are in the avenue. To further study the effect of different TM cations on structural diversity, when the Fe^{3+} cations were replaced by Fe^{2+}, Co^{2+} and Ni^{2+} cations under the same conditions, however, only some amorphous precipitates were isolated. Therefore, TM ions also play an important role in the construction of products. Next, the step by step assembly strategy will be employed in this system. That is, prefabricated TM substituted TA precursors will be used to react with RE cations or prefabricated RE substituted TA precursors will be used to react with TM cations to construct our desired TA-based TM–RE heterometallic derivatives. Certainly, the pH of the solution is a key factor; when the pH was approximately adjusted to 0.5, the products were obtained. However, the systemic development on TA-based TM–RE heterometallic derivatives still remains a great difficulty for us. In the future, we will continuously explore and discover novel extended PTRHDs by changing different synthetic conditions including pH, temperature and reactants.

Structural descriptions

1–5 were all prepared *via* a similar conventional aqueous solution method and the common structural characteristic of 1–5 is that they include a tetra-Fe^{III} substituted Krebs-type sandwich $[Fe_4(H_2O)_{10}(B\text{-}\beta\text{-}SbW_9O_{33})_2]^{6-}$ unit, which is constructed from two trilacunary Keggin subunits $[B\text{-}\beta\text{-}SbW_9O_{33}]^{9-}$ encapsulating a rhomb-like $\{Fe^{III}_4\}$ cluster. In the $[Fe_4(H_2O)_{10}(B\text{-}\beta\text{-}SbW_9O_{33})_2]^{6-}$ unit, the Fe and W atoms can be unambiguously determined by checking their anisotropic thermal displacement parameters and the Fe–O or W–O distances. This unambiguous determination of the 3d-metal and W atom in tetra-TM substituted Krebs-type sandwich POMs is very common.[5,6,13] In addition, the phase purity of 1–5 is determined by the consistency of the experimental PXRD patterns of the as-prepared samples with the XRD patterns obtained from the single-crystal X-ray diffraction (Fig. 1).

1 crystallizes in the triclinic space group $P\bar{1}$ and its structural unit consists of a sandwich-type $[Fe_4(H_2O)_{10}(B\text{-}\beta\text{-}SbW_9O_{33})_2]^{6-}$ POA and two crystallographically independent Pr^{3+} cations (Fig. 2a). The sandwich-type $[Fe_4(H_2O)_{10}(B\text{-}\beta\text{-}SbW_9O_{33})_2]^{6-}$ POA can be simplified into two cages encapsulating a $\{Fe^{III}_4\}$ belt (Fig. 2b). The well-known sandwich-type $[Fe_4(H_2O)_{10}(B\text{-}\beta\text{-}SbW_9O_{33})_2]^{6-}$ POA is composed of two trivacant Keggin $[B\text{-}\beta\text{-}SbW_9O_{33}]^{9-}$ building blocks in a staggered fashion sandwiching a central symmetric rhomb-like $\{Fe^{III}_4\}$ group, in which the four Fe^{III} cations lie at the corners of a rhombus with adjacent two edges of 5.656 and 5.664 Å; meanwhile, adjacent Fe^{III} cations are bridged by the Fe–O–W–O–Fe bonds, and the distance of two inner Fe···Fe is 5.408 Å while the distance of two external Fe···Fe is 9.945 Å (Fig. 3). This connection mode is somewhat distinct from that in the

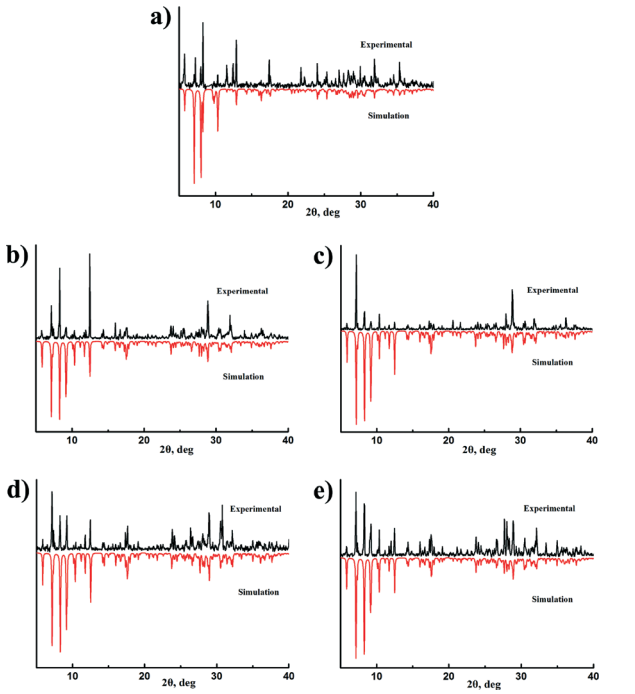

Fig. 1 (a) The experimental PXRD and simulated XRD patterns of the as-prepared 1. (b) The experimental PXRD and simulated XRD patterns of the as-prepared 2. (c) The experimental PXRD and simulated XRD patterns of the as-prepared 3. (d) The experimental PXRD and simulated XRD patterns of the as-prepared 4. (e) The experimental PXRD and simulated XRD patterns of the as-prepared 5.

tetra-Fe^{III} sandwiched unit $[Fe_4(en)(B\text{-}\alpha\text{-}GeW_9O_{34})_2]^{8-}$ reported by our group recently,[30] in which four Fe^{III} centers are connected by Fe–O–Fe bonds. Nevertheless, the sandwich belt of the POA in 1 is defined by two types of inequivalent Fe^{III} cations, which contain two interior Fe^{III} ions (Fe2 and Fe2A) and two exterior Fe^{III} cations (Fe1 and Fe1A). Albeit two types of Fe^{III} cations display the octahedral geometries, their coordination surroundings are somewhat different. The octahedral $Fe2^{III}$ cation is defined by two O atoms from one $[B\text{-}\beta\text{-}SbW_9O_{33}]^{9-}$ fragment [Fe–O: 1.956(10)–1.971(11) Å], two

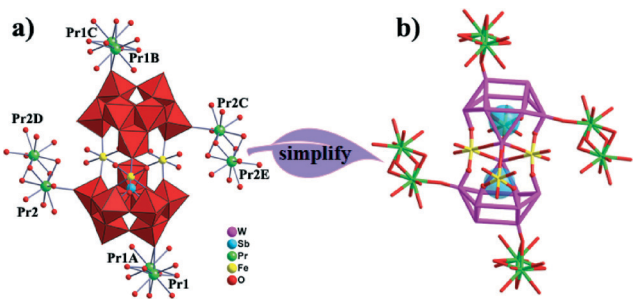

Fig. 2 (a) Polyhedral/ball-and-stick representation of the structural unit of 1. Lattice water molecules are omitted for clarity. The atoms with the suffix A, B, C, D, and E are generated by the symmetry operation: A: $-x, 1-y, 2-z$; B: $1+x, 1+y, -1+z$; C: $1-x, 2-y, 1-z$; D: $-x, 3-y, 1-z$; E: $1+x, -1+y, z$. (b) The simplified view of the structural unit of 1.

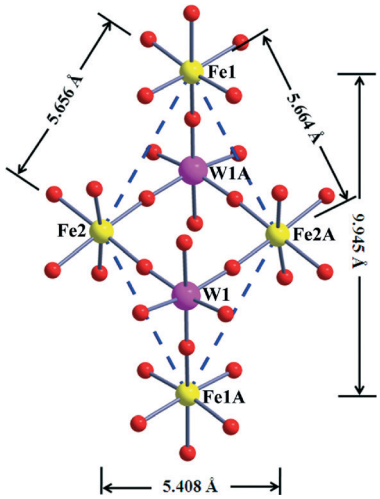

Fig. 3 The central symmetric rhomb-like $\{Fe^{III}_4\}$ group in **1** showing the Fe···Fe distances. The atoms with the suffix A are generated by the symmetry operation: A: 1 − *x*, 2 − *y*, 1 − *z*.

O atoms from the other $[B\text{-}\beta\text{-}SbW_9O_{33}]^{9-}$ fragment [Fe–O: 1.918(11)–1.963(10) Å] and two O atoms from two terminal H_2O ligands [Fe–O: 2.087(11)–2.089(13) Å], whereas the octahedral $Fe1^{III}$ cation is built by two O atoms from one $[B\text{-}\beta\text{-}SbW_9O_{33}]^{9-}$ fragment [Fe–O: 1.906(11)–1.941(11) Å], one O atom from the other $[B\text{-}\beta\text{-}SbW_9O_{33}]^{9-}$ fragment [Fe–O: 1.972(10) Å] and three O atoms from three terminal H_2O ligands [Fe–O: 2.034(11)–2.098(14) Å]. It is interesting that each sandwich-type dimeric $[Fe_4(H_2O)_{10}(B\text{-}\beta\text{-}SbW_9O_{33})_2]^{6-}$ POA is combined with the four adjacent same ones alternatively by O–Pr–O bonds resulting in a unique 2-D sheet architecture (Fig. 4a). However, the linkers are defined by two types of inequivalent Pr^{III} (Pr1 and Pr2) ions. The $Pr1^{III}$ cation coordinates directly to the terminal atom that is away from the sandwich belt of the $[Fe^{III}_4(H_2O)_{10}(B\text{-}\beta\text{-}SbW_9O_{33})_2]^{6-}$ POA; what's more, the $Pr1^{III}$ cation is disordered over two positions (Pr1 and Pr1A) with a site occupancy of 50% for each position and the Pr···Pr distance is 1.842(4) Å. The $Pr1^{III}$ cation exhibits an eight-coordinate severely distorted square antiprismatic configuration [Pr–O: 2.518(11)–2.72(4) Å]. The $Pr1^{III}$ cations can be viewed as connectors that link the sandwich-type POAs into an infinite 1-D chain. The $Pr2^{III}$ cation links to the terminal O atom near the sandwich belt of the $[Fe^{III}_4(H_2O)_{10}(B\text{-}\beta\text{-}SbW_9O_{33})_2]^{6-}$ POA, and it is also disordered over two positions (Pr2 and Pr2D) with the site occupancy of 50% for each position and the Pr···Pr distance is 3.102(6) Å. Nevertheless, the $Pr2^{III}$ cation displays a nine-coordinate monocapped square antiprism configuration [Pr–O: 2.36(2)–2.62(5) Å], and the $Pr2^{III}$ cations function as connectors to join neighboring 1-D chains further into a 2-D sheet construction (Fig. 4a, b). As illustrated in Fig. 4c, adjacent 2-D sheets are regularly aligned in a staggered pattern to reduce the steric hindrance. As far as we know, **1** represents the first 2-D extended sheet constructed from the tetra-Fe^{III} substituted sandwich-type units $[Fe_4(H_2O)_{10}(B\text{-}\beta\text{-}SbW_9O_{33})_2]^{6-}$ through Pr^{III} linkers. From a topology viewpoint, supposing

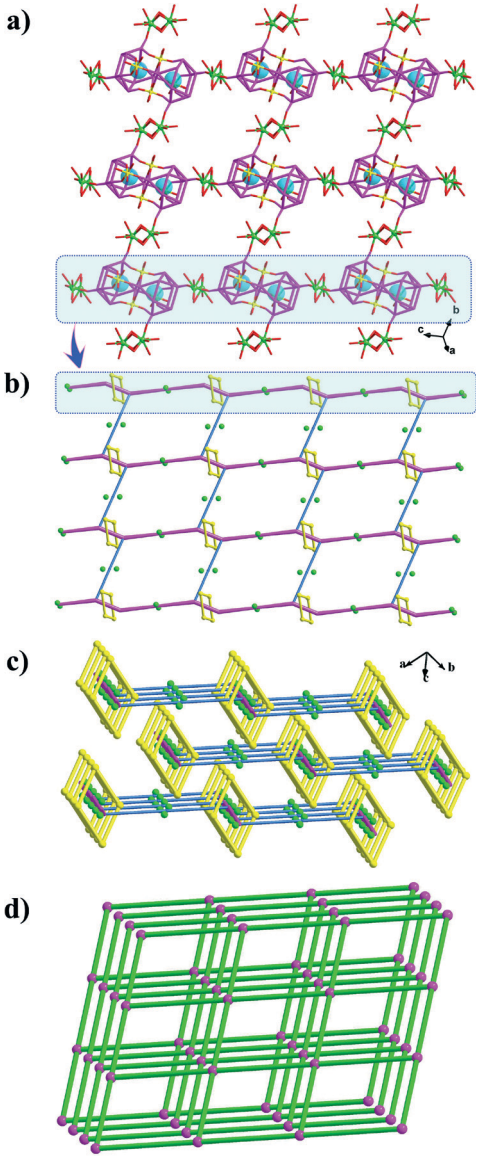

Fig. 4 (a) The 2-D sheet architecture constructed from $[Fe_4(H_2O)_{10}(B\text{-}\beta\text{-}SbW_9O_{33})_2]^{6-}$ POAs and Pr^{III} linkers in **1**. Lattice water molecules are omitted for clarity. (b) The simplified schematic view of the 2-D sheet, in which yellow rhombs represent $\{Fe^{III}_4\}$ groups and green balls stand for disordered Pr^{III} cations. (c) The packing of schematic 2-D sheets exhibiting a staggered pattern to reduce the steric hindrance. (d) The 2-D (4,4) topological sheet.

that the structural unit of $[Pr(H_2O)_8][Pr(H_2O)_6][Fe_4(H_2O)_{10}(B\text{-}\beta\text{-}SbW_9O_{33})_2]$ is considered as a four-connected node, the 2-D sheet of **1** facilitates a 2-D (4,4)-network topology (Fig. 4d). As a result, the discovery of **1** offers us a useful guidance for the development of the complicated inorganic or organic–inorganic coordination networks of TA-based TM–RE heterometallic derivatives.

To our knowledge, the well-known highly charged trivacant species $[SbW_9O_{33}]^{9-}$ is obtained by removal of three edge-sharing WO_6 octahedra of a hypothetical parent Keggin anion, which can be depicted as the combination of three $\{W_3O_{13}\}$ groups around the $\{SbO_3\}$ central pyramid and

possesses two isomers B-α and B-β. Formally, the [B-β-SbW_9O_{33}]$^{9-}$ anion can be envisioned as an isomer of the [B-α-SbW_9O_{33}]$^{9-}$ anion; that is, the 60° rotation of one edge-shared {W_3O_{13}} group in the [B-α-SbW_9O_{33}]$^{9-}$ anion generates the [B-β-SbW_9O_{33}]$^{9-}$ anion. It should be noted that the sandwich-type [$Fe_4(H_2O)_{10}$(B-β-SbW_9O_{33})$_2$]$^{6-}$ POA presented in **1** contains two [B-β-SbW_9O_{33}]$^{9-}$ building blocks. However, the [B-β-SbW_9O_{33}]$^{9-}$ fragment was not used as the starting material during the preparation of **1**; therefore, the isomerization of B-α → B-β of the [SbW_9O_{33}]$^{9-}$ unit must have occurred. The conceivable reaction process is similar to that reported by Krebs.[4] The precursor [B-α-SbW_9O_{33}]$^{9-}$ is obtained in a basic medium; when the reaction medium is changed to be acidic, the precursor [B-α-SbW_9O_{33}]$^{9-}$ has a higher tendency to isomerize to the [B-β-SbW_9O_{33}]$^{9-}$ fragment.[4,31] This is in good accordance with the synthetic conditions for **1**, which was obtained at pH 0.5. Such isomerization phenomenon has been reported in previous research on TAs, as listed in Table S1.†[32] **2**–**5** are isostructural and belong to the triclinic space group $P\bar{1}$; therefore, only **2** is discussed in detail herein. Although they were obtained in the same system as **1**, their structural constructions are somewhat different. On one hand, the common characteristic of the sandwich-type [$Fe_4(H_2O)_{10}$(B-β-SbW_9O_{33})$_2$]$^{6-}$ POAs in **1** and **2** is that they can be described as two trivacant Keggin [B-β-SbW_9O_{33}]$^{9-}$ units sandwiching a central symmetric {Fe^{III}_4} segment, resulting in the classic sandwich-type assembly. On the other hand, four striking differences between them can be found: (a) there are two crystallographically unique Pr^{III} cations in **1**; in contrast, only one crystallographically independent Tb^{III} cation is observed in **2**; (b) the coordination positions of RE cations on the surfaces of [B-β-SbW_9O_{33}]$^{9-}$ units are differentiated: in **1**, two types of Pr^{III} cations are simultaneously combined with the terminal O atoms that are away from and near the sandwich belt of the [$Fe^{III}_4(H_2O)_{10}$(B-β-SbW_9O_{33})$_2$]$^{6-}$ POA; on the contrary, in **2**, the Tb^{III} cations link to terminal O atoms that are adjacent to the sandwich belt of POA (Fig. 5a); (c) each Pr^{III} cation in **1** is disordered over two positions with a site occupancy of 50% for each position while the Tb^{III} cation in **2** is completely localized with a site occupancy of 100%; (d) **1** shows a 2-D sheet architecture, whereas **2** employs a discrete structure. In addition, the [$Tb(H_2O)_7$]$_2$[$Fe_4(H_2O)_{10}$(B-β-SbW_9O_{33})$_2$] entities in **2** are regularly arranged in the –AAA– motif along the *b* or *c* axis (Fig. 5b).

It is obvious that **1**–**5** all consist of tetra-Fe^{III} substituted dimeric sandwich-type [$Fe^{III}_4(H_2O)_{10}$(B-β-SbW_9O_{33})$_2$]$^{6-}$ POAs as the fundamental building blocks. This tetra-Fe^{III} substituted Krebs-type sandwich POA [$Fe^{III}_4(H_2O)_{10}$(B-β-SbW_9O_{33})$_2$]$^{6-}$ (**A**) is comparable to the tetra-Fe^{III} substituted Weakley's sandwich-type POA [$Fe^{III}_4(H_2O)_2$(B-α-$Fe^{III}W_9O_{34}$)$_2$]$^{10-}$ (**B**) that was reported by Niu's group in 2013 (Fig. 6).[33] The common feature of **A** and **B** is that they were prepared by making use of Na_9[B-α-SbW_9O_{33}]·19.5H_2O and can be viewed as two trivacant Keggin-type fragments anchoring a tetra-Fe^{III} core illustrating the classic sandwich-type subfamily. Although **A** is somewhat similar to the **B**, the main

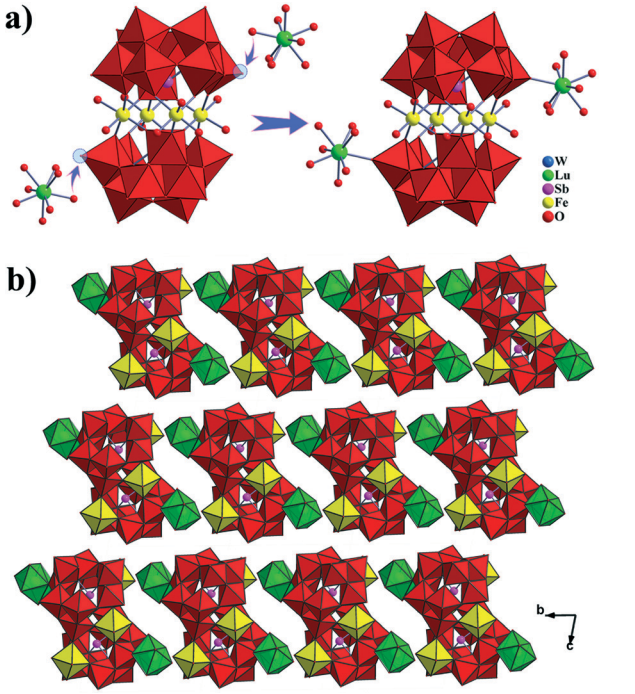

Fig. 5 (a) Polyhedral/ball-and-stick representation of the structural unit of **2**. (b) The packing view of **2** in the *bc* plane. Lattice water molecules are omitted for clarity.

discrepancies between **A** and **B** rest on three aspects: (1) the synthetic methods are discrepant: **A** was synthesized under the conventional aqueous solution while **B** was separated under the hydrothermal conditions; (2) the differences of the trivacant Keggin-type fragments give rise to the imparities of their structures: **A** contains two [B-β-SbW_9O_{33}]$^{9-}$ fragments with the presence of a lone pair of electrons on the tri-coordinate Sb^{III} heteroatom, whereas **B** includes two [B-α-FeW_9O_{34}]$^{11-}$ fragments with the four-coordinate Fe^{III} heteroatom; (3) the greatest differences between them are that **A** contains a rhomb-like tetra-Fe^{III} group, in which adjacent Fe^{III} cations are bridged by the Fe–O–W–O–Fe bonds; however, adjacent Fe^{III} cations are

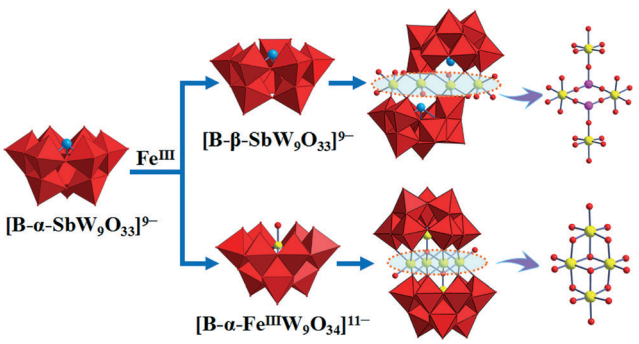

Fig. 6 The comparison of the tetra-Fe^{III} substituted Krebs' sandwich-type [$Fe^{III}_4(H_2O)_{10}$(B-β-SbW_9O_{33})$_2$]$^{6-}$ in **1**–**5** and the previously reported tetra-Fe^{III} substituted Weakley's sandwich-type POA [$Fe^{III}_4(H_2O)_2$(B-α-$Fe^{III}W_9O_{34}$)$_2$]$^{10-}$.

joined by the Fe–O–Fe bonds in **B**. Moreover, comparing **1–5** with $[RE(H_2O)_8]_2[Fe_4(H_2O)_8(thr)_2](B\text{-}\beta\text{-}SbW_9O_{33})_2]\cdot 22H_2O$ (RE = Pr^{III}, Nd^{III}, Sm^{III}, Eu^{III}, Gd^{III}, Dy^{III}, Lu^{III}) reported by us in 2014, two obvious differences in synthetic methods and structures can be observed: (1) the pH of the reaction system of **1–5** is controlled at *ca.* 0.5, whereas the pH of the reaction solution of $[RE(H_2O)_8]_2[Fe_4(H_2O)_8(thr)_2][B\text{-}\beta\text{-}SbW_9O_{33}]_2\cdot 22H_2O$ is adjusted to *ca.* 1.2; (2) **1** displays the inorganic 2-D extended sheet built by tetra-Fe^{III} sandwich-type units $[Fe_4(H_2O)_{10}(B\text{-}\beta\text{-}SbW_9O_{33})_2]^{6-}$ *via* Pr^{3+} linkers, **2–5** exhibit the inorganic isolated structure based on $[Fe_4(H_2O)_{10}(B\text{-}\beta\text{-}SbW_9O_{33})_2]^{6-}$ with two supporting $[RE(H_2O)_7]^{3+}$ cations on the top and bottom sides, while $[RE(H_2O)_8]_2[Fe_4(H_2O)_8(thr)_2(B\text{-}\beta\text{-}SbW_9O_{33})_2]\cdot 22H_2O$ adopt the isolated organic–inorganic hybrid architecture functionalized by amino acid ligands, in which two thr ligands substitute for two water ligands of the classic $[Fe_4(H_2O)_{10}(B\text{-}\beta\text{-}SbW_9O_{33})_2]^{6-}$ POA leading to the $[Fe_4(H_2O)_8(thr)_2(B\text{-}\beta\text{-}SbW_9O_{33})_2]^{6-}$ hybrid unit.

Furthermore, to the best of our knowledge, tetranuclear TM substituted sandwich-type POMs mainly comprise other seven kinds of structural types as well as the above-mentioned Weakley- and Krebs-type structures (Fig. 7). In 2006, Kortz's group published an asymmetric dimeric species $[Zr_4O_2(OH)_2(H_2O)_4(\beta\text{-}SiW_{10}O_{37})_2]^{10-}$ consisting of β_{22}- and β_{12}-$SiW_{10}O_{37}$ segments sandwiching a $[Zr_4O_2(OH)_2(H_2O)_4]^{10+}$ cluster (Fig. 7a).[34] In the same year, Mizuno *et al.* synthesized an unexpected cyclic tetra-Ti^{IV} substituted silicotungstate $[\{\gamma\text{-}SiTi_2W_{10}O_{36}(OH)_2\}_2(\mu\text{-}O)_2]^{8-}$ (Fig. 7b).[35] Subsequently, Hill and co-workers prepared a highly active tetraruthenium homogeneous catalyst for water oxidation $[\{Ru^{IV}_4O_4(OH)_2(H_2O)_4\}(\gamma\text{-}SiW_{10}O_{36})_2]^{10-}$, in which two staggered $[\gamma\text{-}SiW_{10}O_{36}]^{8-}$ fragments incorporate an adamantane-like $[Ru^{IV}_4(\mu\text{-}O)_4(\mu\text{-}OH)_2(H_2O)_4]^{6+}$ core (Fig. 7c).[36] Meanwhile, Dolbecq's group obtained a unique phosphotungstate $[(PW_{11}O_{39})_2Fe_4^{III}O_2(dmbpy)_4]^{6-}$ with a butterfly-like tetra-Fe^{III} $[Fe_4^{III}O_2(dmbpy)_4]^{8+}$ hybrid cluster encapsulated between two monolacunary $[\alpha\text{-}PW_{11}O_{39}]^{7-}$ segments (Fig. 7d).[37] In 2010, Liu's group reported an acetate-functionalized tetra-Zr sandwiched POM $[Zr_4(OH)_6(CH_3COO)_2(\alpha\text{-}PW_{10}O_{37})_2]^{10-}$ built by two dilacunary $[\alpha\text{-}PW_{10}O_{37}]^{8-}$ subunits linked *via* a $[Zr_4(OH)_6(CH_3COO)_2]^{8+}$ central cluster (Fig. 7e).[38] Recently, Mizuno *et al.* isolated two novel Zinc-containing sandwich-type silicotungstates $[\{Zn_2W(O)O_3\}_2H_4\{\alpha\text{-}SiW_9O_{33}\}_2]^{8-}$ (Fig. 7f) and $[\{Zn_2W(O)O_3\}_2H_4\{\beta\text{-}SiW_9O_{33}\}_2]^{8-}$ (Fig. 7g), which consist of two $[SiW_9O_{33}]^{8-}$ subunits sandwiching the unprecedented distorted hexaprismane core $[\{Zn_2W(O)O_3\}_2]^{4+}$.[39] Simultaneously, they also communicated a tetra-silver substituted sandwich-type silicotungstate $[Ag_4(\gamma\text{-}H_2SiW_{10}O_{36})_2]^{8-}$ constructed from two $[\gamma\text{-}SiW_{10}O_{36}]^{8-}$ subunits encapsulating a diamond-shaped $[Ag_4]^{4+}$ cluster (Fig. 7h).[40]

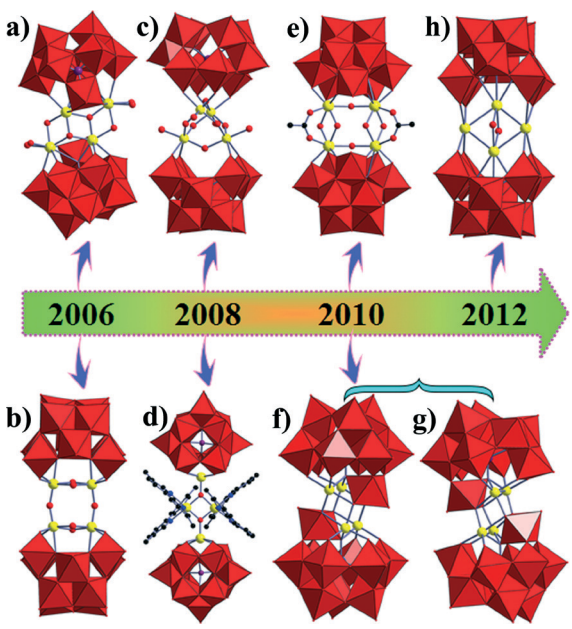

Fig. 7 Illustrations of some representative tetranuclear (a–h) sandwich-type compounds previously reported.

IR spectra

IR spectra for **1–5** were recorded in the range of 4000 and 400 cm^{-1} with KBr pellets (Fig. S1†). In the low-wavenumber region ($\nu < 1000$ cm^{-1}), IR spectra of **1–5** display four similar characteristic vibration patterns derived from the Keggin-type framework observed at 649–662, 952–957, 878–889 and 776–788 cm^{-1}, which are ascribed to ν(Sb–O_a), terminal ν(W–O_t), corner-sharing ν(W–O_b) and edge-sharing ν(W–O_c), respectively. The similarity of IR spectra of **1–5** in the low-wavenumber domain suggests that all of them contain the tetra-Fe^{III} substituted sandwich-type $[Fe_4(H_2O)_{10}(B\text{-}\beta\text{-}SbW_9O_{33})_2]^{6-}$ units in their skeletons. Compared with the IR spectrum of $Na_{10}[B\text{-}\alpha\text{-}SbW_9O_{34}]\cdot 19.5H_2O$ [767, 920, 890 and 715 cm^{-1} for ν(Sb–O_a), ν(W–O_t), ν(W–O_b), and ν(W–O_c) asymmetry stretching vibrations],[4] four characteristic asymmetry vibration peaks for **1–5** have different shifts, which may be assigned to the configuration transformation of $[B\text{-}\alpha\text{-}SbW_9O_{33}]^{9-}$ → $[B\text{-}\beta\text{-}SbW_9O_{33}]^{9-}$ and the implanting of the rhomb-like $\{Fe^{III}_4\}$ cluster to the vacant sites of two $[B\text{-}\beta\text{-}SbW_9O_{33}]^{9-}$ fragments. Furthermore, these IR data are comparable to those of the dimeric Krebs' structure $Na_6[Fe_4(H_2O)_{10}(B\text{-}\beta\text{-}SbW_9O_{33})_2]\cdot 32H_2O$ [678, 948, 883 and 773 cm^{-1} for ν(Sb–O_a), ν(W–O_t), ν(W–O_b) and ν(W–O_c) asymmetry stretching vibrations];[13] four characteristic asymmetry vibration bands for **1–5** only have little shifts, indicating that RE cations have certain effect on $[Fe_4(H_2O)_{10}(B\text{-}\beta\text{-}SbW_9O_{33})_2]^{6-}$ POAs.

Electrochemical and electrocatalytic properties

To survey their electrochemical and electrocatalytic properties, the cyclic voltammetry (CV) measurements of **1** and **2** were carried out in 0.5 mol L^{-1} H_2SO_4 + Na_2SO_4 aqueous solution. Both compounds display similar electrochemical (Fig. 8, S2, and S3†) and electrocatalytic properties, which may result from the same POA building unit $[Fe^{III}_4(H_2O)_{10}(B\text{-}\beta\text{-}SbW_9O_{33})_2]^{6-}$ in their structures of **1** and **2**. The reproducibility of cyclic voltammograms is indicative of the stability of **1** and **2** in this medium (Fig. S4†).

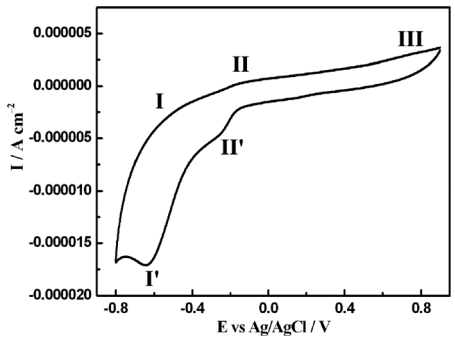

Fig. 8 Cyclic voltammogram of **1** (concentration: 1.73 × 10^{-4} mol L^{-1}) in 0.5 mol L^{-1} Na_2SO_4 + H_2SO_4 aqueous solution (pH = 1.44). Scan rate: 30 mV s^{-1}.

Fig. 8 demonstrates the typical cyclic voltammogram for **1** (at a concentration of 1.73 × 10^{-4} mol L^{-1}) dissolved in 0.5 mol L^{-1} H_2SO_4 + Na_2SO_4 aqueous solution, pH = 1.44, at a scan rate of 30 mV s^{-1}. The typical cyclic voltammogram for **2** is illustrated in Fig. S3a.† In the negative potential direction, the cyclic voltammogram exhibits two pairs of redox waves with the corresponding $E_{1/2}$ peak potentials located at −0.566 V (I/I′) and −0.197 V (II/II′) for **1** and −0.550 V (I/I′) and −0.185 V (II/II′) for **2** [$E_{1/2}$ = (E_{pa} + E_{pc})/2], respectively. In the positive potential direction, there is only an ill-defined oxidation peak appearing at +0.749 V (III) for **1** and +0.734 V (III) for **2**, and the corresponding reduction peak is not readily visible. As expected, the W^{VI}-based waves are seen at the more negative potential than the Fe^{III}-based wave. The ΔE_p values of two couples of redox waves (I–I′ and II–II′) in the cyclic voltammograms are 178 mV and 100 mV for **1** and 223 mV and 107 mV for **2**, respectively (Tables S2, S3†), which suggest the quasi-reversible redox processes of W^{VI} centers in the POA frameworks (the theoretical value of the ΔE_p value for a reversible one-electron transfer process is about 59 mV). These results are in accordance with the previous documents.[41] The appearance of a single oxidation peak potential at +0.749 V (III) for **1** and +0.734 V (III) for **2** confirms the irreversible process of the Fe^{III} centers.[42] The related discussion on the influences of the scan rate and the pH on the electrochemical behaviors of **1** and **2** are shown in the ESI† (Fig. S2, S3, S5, S6, and S7; Tables S2 and S3).

As is well known, electrocatalytic properties of POMs have been widely explored on account of their capability of delivering the electrons to other species and experiencing rapid multi-electron transfer redox processes.[43] Some groups have been working on the exploration of the electrocatalytic reductions of POMs (such as Mialane, Dolbecq, Kortz and Wang and so on).[43,44] Inspired by the previous excellent work, we have also done some research on electrocatalytic properties. Recently, our group reported that two novel Cu^{II}–RE^{III} heterometallic germanotungstate hybrids had obvious electrocatalytic activities toward nitrite and bromate and a Fe^{III}–Pr^{III} heterometallic TA hybrid was effective in the electrocatalytic reduction of nitrite, bromate and hydrogen peroxide.[45] Here, **1** and **2** were employed to probe their electrocatalytic activities toward the reduction of nitrite (NO_2^-) and bromate (BrO_3^-) in 0.5 mol L^{-1} Na_2SO_4 + H_2SO_4 aqueous solution, pH 1.44 (Fig. 9 and S8†). As illustrated in Fig. 9a, it can be clearly seen that with the addition of nitrite, the Fe^{III}-based peak current intensity remains almost unvaried, and the cathodic reduction current intensities of two couples of W^{VI}-based waves gradually increase, meanwhile the corresponding anodic oxidation current intensities decrease gradually. Moreover, compared with the first redox couple (I–I′), the second redox couple (II–II′) shows a weak evolution trend. These results indicate that the reduction process of nitrite is mainly controlled by the reduced species of tungsten-oxo clusters in **1**. This phenomenon is in good agreement with the previous reports.[46] Furthermore, the electrocatalytic activity of **1** toward the reduction of bromate was also measured (Fig. 9b), and the electrocatalytic procedure occurs on the first (I–I′) and second (II–II′) redox couples. With the addition of BrO_3^-, the cathodic peak current intensities of two redox couples gradually enhance and the opposite anodic peak current intensities decrease, whereas the Fe^{III}-based wave is almost unaffected by the addition of BrO_3^-. The results indicate that the reduction of bromate is also mainly mediated by the reduced species of tungsten-oxo clusters in **1**. It is apparent that **2** exhibits a similar electrocatalytic behavior toward the reduction of NO_2^- and BrO_3^- (Fig. S8†). In addition, the electrocatalytic activities of $Na_9[B\text{-}\alpha\text{-}SbW_9O_{33}]\cdot 19.5H_2O$, $FeCl_3$

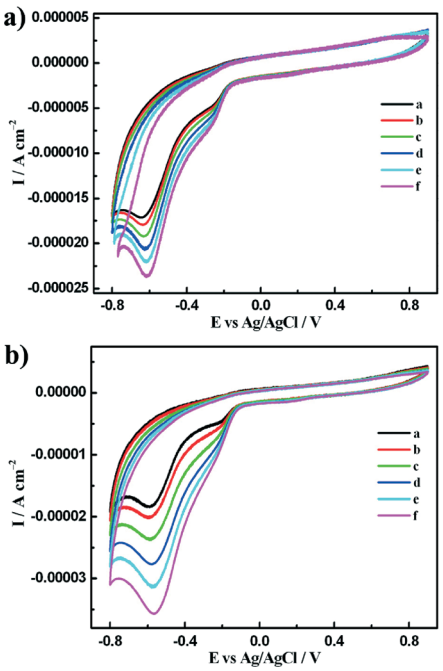

Fig. 9 (a) Cyclic voltammograms of **1** (concentration: 1.73 × 10^{-4} mol L^{-1}) in 0.5 mol L^{-1} Na_2SO_4 + H_2SO_4 aqueous solution, pH = 1.44, with the addition of various concentrations of $NaNO_2$ (a: 0, b: 1 × 10^{-5}, c: 3 × 10^{-5}, d: 7 × 10^{-5}, e: 1 × 10^{-4}, f: 1.5 × 10^{-4} mol L^{-1}). (b) Cyclic voltammograms of **1** (concentration: 1.73 × 10^{-4} mol L^{-1}) in 0.5 mol L^{-1} Na_2SO_4 + H_2SO_4 aqueous solution, pH = 1.44, with the addition of various concentrations of $NaBrO_3$ (a: 0, b: 1 × 10^{-5}, c: 3 × 10^{-5}, d: 5 × 10^{-5}, e: 7 × 10^{-5}, f: 9 × 10^{-5} mol L^{-1}).

·6H_2O, $PrCl_3$·6H_2O and $TbCl_3$·6H_2O toward the reduction of NO_2^- and BrO_3^- were also performed under similar conditions (Fig. S9–S12†). The results show that Na_9[B-α-SbW_9O_{33}]·19.5H_2O exhibits very weak electrocatalytic activities toward the reduction of NO_2^- and BrO_3^- under similar conditions (Fig. S9†). As shown in Fig. S10,† $FeCl_3$·6H_2O has almost no electrocatalytic activity toward the reduction of NO_2^-, whereas it illustrates weak electrocatalytic activity toward the reduction of BrO_3^-. As expected, both $PrCl_3$·6H_2O and $TbCl_3$·6H_2O have no electrocatalytic activities toward the reduction of NO_2^- and BrO_3^- (Fig. S11 and S12†). These comparative experiments further confirm that the electrocatalytic activities of **1** and **2** toward the reduction of nitrite and bromate are mainly controlled by tungsten-oxo cluster fragments in their structures. However, the electrocatalytic activities of **1** and **2** that are better than Na_9[B-α-SbW_9O_{33}]·19.5H_2O may be derived from the synergistic contribution of $[B\text{-}\beta\text{-}SbW_9O_{33}]^{9-}$ and $\{Fe^{III}{}_4\}$ segments, which suggests that the incorporation of TM cations into lacunary polyoxotungstate matrices can improve the electrocatalytic activities. According to the method introduced by Keita, we can estimate and compare the catalytic efficiency (CAT) of **1** and **2** for the reduction of nitrite and bromate. Take $NaNO_2$ for example, the CAT of I′ is defined by: CAT = 100 × {I_p(POM, $NaNO_2$)–I_p(POM)}/I_p(POM) where I_p(POM) and I_p(POM, $NaNO_2$) are the cathodic peak current intensities in the absence and in the presence of $NaNO_2$, respectively.[47] In Table S4,† the CAT values of the first W reduction peak (I′) for **1** and **2** (catalyst, 1.47 × 10^{-4} mol L^{-1}) with regard to 1 × 10^{-5} mol L^{-1} $NaNO_2$ are calculated to be 4.78% and 4.55%; with regard to 3 × 10^{-5} mol L^{-1} $NaNO_2$, the values are calculated to be 12.07% and 9.89%; with regard to 1.5 × 10^{-4} mol L^{-1} $NaNO_2$, the values are calculated to be 38.08% and 29.31%, respectively. Obviously, the results demonstrate that the CAT of **1** is slightly higher than **2** in the electrocatalytic reduction of nitrite. Table S5† displays the CAT values of **1** and **2** for the bromate reduction; it is evident that the CAT of **1** is also slightly higher than **2** in the electrocatalytic reduction of BrO_3^-. However, under the same conditions, the catalytic activities of **1** and **2** in the reduction of BrO_3^- are higher than that of NO_2^- (Fig. 9 and S8†).

TG analyses

The thermal stability of **1–5** has been investigated on crystalline samples under a nitrogen atmosphere from 25 to 750 °C. The TG curves indicate that **1–5** undergo a slow one-step weight loss process (Fig. 10). For **1**, the weight loss of 13.26% involves the loss of 16 lattice water molecules and 24 coordination water molecules (calcd. 12.34%). The weight loss of 14.18%, 14.46%, 14.37% and 14.82% for **2**, **3**, **4** and **5** corresponds to the loss of 22 lattice water molecules and 24 coordination water molecules (calcd. 13.85%, 13.83%, 13.78%, and 14.18%, respectively).

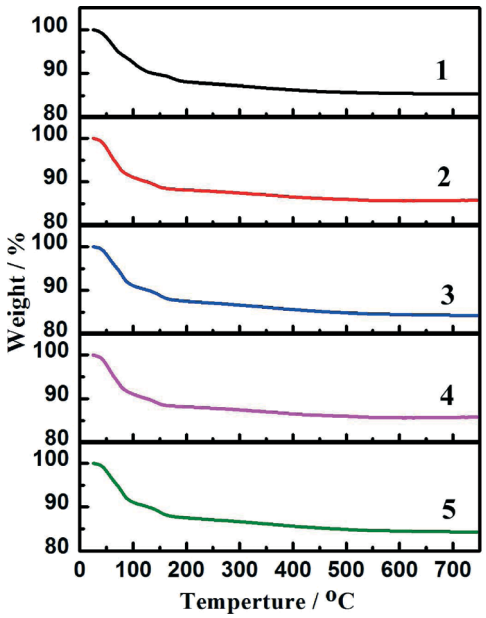

Fig. 10 The TG curves of **1–5**.

Conclusions

Two types of novel purely inorganic TA-based Fe–RE heterometallic derivatives have been successfully separated under the conventional aqueous solution method and structurally characterized by elemental analysis, IR spectroscopy, PXRD, single-crystal X-ray diffraction and TG analysis. **1–5** represent the first purely inorganic Fe–RE heterometallic TAs based on tetra-Fe^{III} substituted sandwich-type $[Fe_4(H_2O)_{10}(B\text{-}\beta\text{-}SbW_9O_{33})_2]^{6-}$ POAs. Furthermore, other types of tetra-TM sandwiched POMs have been summarized and compared. In addition, the electrochemical and electrocatalytic properties of **1** and **2** have been evaluated in aqueous media. Both **1** and **2** manifest obvious electrocatalytic activity toward the reduction of NO_2^- and BrO_3^-. The successful syntheses of these heterometallic compounds will provide us with a new opportunity for further searching and finding novel purely inorganic TA-based TM–RE heterometallic derivatives. In the next work, we will utilize prefabricated TM substituted TA precursors to react with RE cations or prefabricated RE substituted TA precursors to react with TM cations to design and prepare desired TA-based TM–RE heterometallic derivatives with interesting structures and unique properties by making use of different TM and RE pairs and different synthetic strategies. We believe that many more TA-based TM–RE heterometallic derivatives will be discovered by means of the step by step assembly strategy. Moreover, implanting polycarboxylic ligands to TM or RE centers in this reaction system to construct organic–inorganic hybrid TA-based TM–RE heterometallic derivatives is also our other goal during the course of our PTRHD exploration.

Acknowledgements

The authors acknowledge the support from the Natural Science Foundation of China (21301049, U1304208), the 2014 Special Foundation for Scientific Research Project of Henan University, the Natural Science Foundation of Henan Province

(122300410106), the Foundation of State Key Laboratory of Structural Chemistry (20120013), the 2012 Young Backbone Teachers Foundation from Henan Province (2012GGJS-027) and the 2013, 2014 Students Innovative Pilot Plans of Henan University.

References

1 (*a*) X. Fang, P. Kögerler, Y. Furukawa, M. Speldrich and M. Luban, *Angew. Chem., Int. Ed.*, 2011, **50**, 5212; (*b*) M. V. Vasylyev and R. Neumann, *J. Am. Chem. Soc.*, 2004, **126**, 884; (*c*) U. Kortz, A. Müller, J. van Slageren, J. Schnack, N. S. Dalal and M. Dressel, *Coord. Chem. Rev.*, 2009, **253**, 2315; (*d*) J. D. Compain, P. Mialane, A. Dolbecq, I. M. Mbomekallé, J. Marrot, F. Sécheresse, E. Rivière, G. Rogez and W. Wernsdorfer, *Angew. Chem., Int. Ed.*, 2009, **48**, 3077; (*e*) S. G. Mitchell, C. Streb, H. N. Miras, T. Boyd, D. L. Long and L. Cronin, *Nat. Chem.*, 2010, **2**, 308; (*f*) A. Müller and S. Roy, *Coord. Chem. Rev.*, 2003, **245**, 153; (*g*) D. L. Long, R. Tsunashima and L. Cronin, *Angew. Chem., Int. Ed.*, 2010, **49**, 1736.

2 T. J. R. Weakley, H. T. J. Evans, J. S. Showell, G. F. Tourné and C. M. Tourné, *J. Chem. Soc., Chem. Commun.*, 1973, 139.

3 J. Fischer, L. Richard and R. Weiss, *J. Am. Chem. Soc.*, 1976, **98**, 3050.

4 M. Bösing, I. Loose, H. Pohlmann and B. Krebs, *Chem. – Eur. J.*, 1997, **3**, 1232.

5 I. Loose, E. Droste, M. Bösing, H. Pohlmann, M. H. Dickman, C. Rosu, M. T. Pope and B. Krebs, *Inorg. Chem.*, 1999, **38**, 2688.

6 M. Piepenbrink, E. M. Limanski and B. Krebs, *Z. Anorg. Allg. Chem.*, 2002, **628**, 1187.

7 D. Laurencin, R. Villanneau, P. Herson, R. Thouvenot, Y. Jeannin and A. Proust, *Chem. Commun.*, 2005, 5524.

8 L. H. Bi, G. Al-Kadamany, E. V. Chubarova, M. H. Dickman, L. F. Chen, D. S. Gopala, R. M. Richards, B. Keita, L. Nadjo, H. Jaensch, G. Mathys and U. Kortz, *Inorg. Chem.*, 2009, **48**, 10068.

9 L. H. Bi, B. Li, S. Bi and L. X. Wu, *J. Solid State Chem.*, 2009, **182**, 1401.

10 L. C. Zhang, H. Xue, Z. M. Zhu, Q. X. Wang, W. S. You, Y. G. Li and E. B. Wang, *Inorg. Chem. Commun.*, 2010, **13**, 609.

11 I. V. Kalinina, N. V. Izarova and U. Kortz, *Inorg. Chem.*, 2012, **51**, 7442.

12 C. C. Zhao, C. S. Kambara, Y. Yang, A. L. Kaledin, D. G. Musaev, T. Q. Lian and C. L. Hill, *Inorg. Chem.*, 2013, **52**, 671.

13 U. Kortz, M. G. Savelieff, B. S. Bassil, B. Keita and L. Nadjo, *Inorg. Chem.*, 2002, **41**, 783.

14 M. Carraro, B. S. Bassil, A. Sorarù, S. Berardi, A. Suchopar, U. Kortz and M. Bonchio, *Chem. Commun.*, 2013, **49**, 7914.

15 (*a*) B. Artetxe, S. Reinoso, L. S. Felices, P. Vitoria, A. Pache, J. Martín-Caballero and J. M. Gutierrez-Zorrilla, *Inorg. Chem.*, 2015, **54**, 241; (*b*) B. Artetxe, S. Reinoso, L. S. Felices, L. Lezama, A. Pache, C. Vicent and J. M. Gutierrez-Zorrilla, *Inorg. Chem.*, 2015, **54**, 409.

16 T. McGlone, L. Vilà-Nadal, H. N. Miras, D.-L. Long, J. M. Poblet and L. Cronin, *Dalton Trans.*, 2010, **39**, 11599.

17 A. J. Gaunt, I. May, R. Copping, A. I. Bhatt, D. Collison, O. D. Fox, K. T. Holman and M. T. Pope, *Dalton Trans.*, 2003, 3009.

18 (*a*) P. Mialane, J. Marrot, E. Rivière, J. Nebout and G. Herve, *Inorg. Chem.*, 2001, **40**, 44; (*b*) U. Kortz, N. K. Al-Kassem, M. G. Savelieff, N. A. Al Kadi and M. Sadakane, *Inorg. Chem.*, 2001, **40**, 4742; (*c*) D. Volkmer, B. Bredenkötter, J. Tellenbröker, P. Kögerler, D. G. Kurth, P. Lehmann, H. Schnablegger, D. Schwahn, M. Piepenbrink and B. Krebs, *J. Am. Chem. Soc.*, 2002, **124**, 10489; (*d*) A. C. Stowe, S. Nellutla, N. S. Dalal and U. Kortz, *Eur. J. Inorg. Chem.*, 2004, 3792; (*e*) L. H. Bi, M. Reicke, U. Kortz, B. Keita, L. Nadjo and R. J. Clark, *Inorg. Chem.*, 2004, **43**, 3915; (*f*) D. Drewes, M. Piepenbrink and B. Krebs, *J. Cluster Sci.*, 2006, **17**, 361; (*g*) R. R. Cui, H. L. Wang, X. Y. Yang, S. H. Ren, H. M. Hu, F. Fu, J. W. Wang and G. L. Xue, *Chin. J. Chem.*, 2007, **25**, 176; (*h*) J. P. Wang, P. T. Ma, J. Li, H. Y. Niu and J. Y. Niu, *Chem. – Asian J.*, 2008, **3**, 822.

19 (*a*) T. Yamase, K. Fukaya, H. Nojiri and Y. Ohshima, *Inorg. Chem.*, 2006, **45**, 7698; (*b*) C. C. Zhao, E. N. Glass, B. Chica, D. G. Musaev, J. M. Sumliner, R. B. Dyer, T. Q. Lian and C. L. Hill, *J. Am. Chem. Soc.*, 2014, **136**, 12085.

20 G. L. Xue, J. Vaissermann and P. Gouzerh, *J. Cluster Sci.*, 2002, **13**, 409.

21 M. Ibrahim, S. S. Mal, B. S. Bassil, A. Banerjee and U. Kortz, *Inorg. Chem.*, 2011, **50**, 956.

22 A. H. Ismail, B. S. Bassil, I. Römer and U. Kortz, *Z. Anorg. Allg. Chem.*, 2013, **639**, 2510.

23 J. W. Zhao, J. Cao, Y. Z. Li, J. Zhang and L. J. Chen, *Cryst. Growth Des.*, 2014, **14**, 6217.

24 G. M. Sheldrick, *SHELXL-97, Program for Crystal Structure Refinement*, University of Göttingen, Göttingen, Germany, 1997.

25 (*a*) B. Li, J.-W. Zhao, S.-T. Zheng and G.-Y. Yang, *Inorg. Chem.*, 2009, **48**, 8294; (*b*) G. L. Xue, B. Liu, H. M. Hu, J. H. Yang, J. W. Wang and F. Fu, *J. Mol. Struct.*, 2004, **690**, 95.

26 (*a*) R. C. Howell, F. G. Perez, S. Jain, W. D. Horrocks, A. L. Rheingold and L. C. Francesconi, *Angew. Chem., Int. Ed.*, 2001, **40**, 4031; (*b*) B. S. Bassil, M. H. Dickman, I. Römer, B. Kammer and U. Kortz, *Angew. Chem., Int. Ed.*, 2007, **46**, 6192; (*c*) S. Yao, Z. M. Zhang, Y. G. Li, Y. Lu, E. B. Wang and Z. M. Su, *Cryst. Growth Des.*, 2010, **10**, 135.

27 S. T. Zheng, M. H. Wang and G. Y. Yang, *Chem. – Asian J.*, 2007, **2**, 1380.

28 W. L. Chen, Y. G. Li, Y. H. Wang and E. B. Wang, *Eur. J. Inorg. Chem.*, 2007, 2216.

29 (*a*) J. F. Cao, S. X. Liu, R. G. Cao, L. H. Xie, Y. H. Ren, C. Y. Gao and L. Xu, *Dalton Trans.*, 2008, 115; (*b*) Z. M. Zhang, Y. G. Li, W. L. Chen, E. B. Wang and X. L. Wang, *Inorg. Chem. Commun.*, 2008, **11**, 879; (*c*) B. Li, J. W. Zhao, S. T. Zheng and G. Y. Yang, *J. Cluster Sci.*, 2009, **20**, 503; (*d*) B. Nohra, P. Mialane, A. Dolbecq, E. Rivière, J. Marrot and F. Sécheresse, *Chem. Commun.*, 2009, 2703; (*e*) D. Y. Du, J. S. Qin, S. L. Li, Y. Q. Lan, X. L. Wang and Z. M. Su, *Aust. J.*

Chem., 2010, **63**, 1389; (*f*) D. Y. Du, J. S. Qin, S. L. Li, X. L. Wang, G. S. Yang, Y. G. Li, K. Z. Shao and Z. M. Su, *Inorg. Chim. Acta*, 2010, **363**, 3823; (*g*) J. D. Compain, P. Mialane, A. Dolbecq, I. M. Mbomekallé, J. Marrot, F. Sécheresse, C. Duboc and E. Rivière, *Inorg. Chem.*, 2010, **49**, 2851; (*h*) J. Y. Niu, S. W. Zhang, H. N. Chen, J. W. Zhao, P. T. Ma and J. P. Wang, *Cryst. Growth Des.*, 2011, **11**, 3769; (*i*) D. Y. Shi, L. J. Chen, J. W. Zhao, Y. Wang, P. T. Ma and J. Y. Niu, *Inorg. Chem. Commun.*, 2011, **14**, 324; (*j*) L. J. Chen, D. Y. Shi, Y. Wang, H. L. Chen, Z. D. Geng, J. W. Zhao, P. T. Ma and J. Y. Niu, *J. Coord. Chem.*, 2011, **64**, 400; (*k*) J. D. Compain, K. Nakabayashi and S. Ohkoshi, *Inorg. Chem.*, 2012, **51**, 4897; (*l*) S. W. Zhang, J. W. Zhao, P. T. Ma, H. N. Chen, J. Y. Niu and J. P. Wang, *Cryst. Growth Des.*, 2012, **12**, 1263; (*m*) S. W. Zhang, J. W. Zhao, P. T. Ma, J. Y. Niu and J. P. Wang, *Chem. – Asian J.*, 2012, **7**, 966; (*n*) D. Y. Shi, J. W. Zhao, L. J. Chen, P. T. Ma, J. P. Wang and J. Y. Niu, *CrystEngComm*, 2012, **14**, 3108; (*o*) H. Y. Zhao, J. W. Zhao, B. F. Yang, H. He and G. Y. Yang, *Cryst. Growth Des.*, 2013, **13**, 5169; (*p*) H. Y. Zhao, J. W. Zhao, B. F. Yang, H. He and G. Y. Yang, *CrystEngComm*, 2013, **15**, 5209; (*q*) Y. Y. Li, J. W. Zhao, Q. Wei, B. F. Yang, H. He and G. Y. Yang, *Chem. – Asian J.*, 2014, **9**, 858.

30 S. B. Tian, Y. Z. Li, J. W. Zhao, P. T. Ma and L. J. Chen, *Inorg. Chem. Commun.*, 2013, **33**, 99.

31 R. X. Tan, X. H. Pang, Y. L. Ren, X. H. Wang and R. Li, *Z. Anorg. Allg. Chem.*, 2011, **637**, 1178.

32 (*a*) A. Dolbecq, J. D. Compain, P. Mialane, J. Marrot, E. Riviere and F. Sécheresse, *Inorg. Chem.*, 2008, **47**, 3371; (*b*) F. Hussain, M. Reicke and U. Kortz, *Eur. J. Inorg. Chem.*, 2004, 2733; (*c*) B. W. Chen, W. L. Chen, Y. G. Li and E. B. Wang, *J. Cluster Sci.*, 2011, **22**, 73.

33 D. D. Zhang, C. Z. Wang, S. Z. Li, J. P. Liu, P. T. Ma, J. P. Wang and J. Y. Niu, *J. Solid State Chem.*, 2013, **198**, 18.

34 B. S. Bassil, M. H. Dickman and U. Kortz, *Inorg. Chem.*, 2006, **45**, 2394.

35 Y. Goto, K. Kamata, K. Yamaguchi, K. Uehara, S. Hikichi and N. Mizuno, *Inorg. Chem.*, 2006, **45**, 2347.

36 Y. V. Geletii, B. Botar, P. Kögerler, D. A. Hillesheim, D. G. Musaev and C. L. Hill, *Angew. Chem., Int. Ed.*, 2008, **47**, 3896.

37 C. Pichon, A. Dolbecq, P. Mialane, J. Marrot, E. Rivière, M. Goral, M. Zynek, T. McCormac, S. A. Borshch, E. Zueva and F. Sécheresse, *Chem. – Eur. J.*, 2008, **14**, 3189.

38 W. Zhang, S. X. Liu, C. D. Zhang, R. K. Tan, F. J. Ma, S. J. Li and Y. Y. Zhang, *Eur. J. Inorg. Chem.*, 2010, 3473.

39 Y. Kikukawa, K. Yamaguchi and N. Mizuno, *Inorg. Chem.*, 2010, **49**, 8194.

40 Y. Kikukawa, Y. Kuroda, K. Yamaguchi and N. Mizuno, *Angew. Chem., Int. Ed.*, 2012, **51**, 2434.

41 (*a*) B. S. Bassil, S. Nellutla, U. Kortz, A. C. Stowe, J. van Tol, N. S. Dalal, B. Keita and L. Nadjo, *Inorg. Chem.*, 2005, **44**, 2659; (*b*) F. Hussain, U. Kortz, B. Keita, L. Nadjo and M. T. Pope, *Inorg. Chem.*, 2006, **45**, 761.

42 (*a*) M. Sadakane and E. Steckhan, *Chem. Rev.*, 1998, **98**, 219; (*b*) U. Kortz, M. G. Savelieff, B. S. Bassil, B. Keita and L. Nadjo, *Inorg. Chem.*, 2002, **41**, 783; (*c*) N. Anwar, M. Vagin, F. Laffir, G. Armstrong, C. Dickinson and T. McCormac, *Analyst*, 2012, **137**, 624.

43 (*a*) Z. G. Han, Y. L. Zhao, J. Peng, Y. H. Feng, J. N. Yin and Q. Liu, *Electroanalysis*, 2005, **17**, 1097; (*b*) B. Nohra, H. E. Moll, L. M. R. Albelo, P. Mialane, J. Marrot, C. Mellot-Draznieks, M. O'Keeffe, R. N. Biboum, J. Lemaire, B. Keita, L. Nadjo and A. Dolbecq, *J. Am. Chem. Soc.*, 2011, **133**, 13363.

44 (*a*) L. H. Bi, U. Kortz, S. Nellutla, A. C. Stowe, J. V. Tol, N. S. Dalal, B. Keita and L. Nadjo, *Inorg. Chem.*, 2005, **44**, 896; (*b*) Z. M. Zhang, Y. F. Qi, C. Qin, Y. G. Li, E. B. Wang, X. L. Wang, Z. M. Su and L. Xu, *Inorg. Chem.*, 2007, **46**, 8162; (*c*) I. M. Mbomekalle, P. Mialane, A. Dolbecq, J. Marrot, F. Sécheresse, P. Berthet, B. Keita and L. Nadjo, *Eur. J. Inorg. Chem.*, 2009, 5194; (*d*) M. Ammam, I. M. Mbomekalle, B. Keita, L. Nadjo, T. M. Anderson, X. Zhang, K. I. Hardcastlec, C. L. Hill and J. Fransaer, *J. Electroanal. Chem.*, 2010, **647**, 97.

45 (*a*) J. W. Zhao, D. Y. Shi, L. J. Chen, P. T. Ma, J. P. Wang, J. Zhang and J. Y. Niu, *Cryst. Growth Des.*, 2013, **13**, 4368; (*b*) J. W. Zhao, Y. Z. Li, F. Ji, J. Yuan, L. J. Chen and G. Y. Yang, *Dalton Trans.*, 2014, **43**, 5694.

46 (*a*) B. Keita, P. de Oliveira, L. Nadjo and U. Kortz, *Chem. – Eur. J.*, 2007, **13**, 5480; (*b*) X. Wang, H. Hu, A. Tian, H. Lin and J. Li, *Inorg. Chem.*, 2010, **49**, 10299.

47 (*a*) B. Keitaa, A. Belhouaria, L. Nadjo and R. Contant, *J. Electroanal. Chem.*, 1995, **381**, 243; (*b*) F. M. Zonoz, I. M. Zonoz, A. Jamshidi and M. H. Alizadeh, *Solid State Sci.*, 2014, **32**, 13.